

Supporting Information

Structural basis for activity of TRIC counter-ion channels in calcium release

Xiao-hui Wang^{a,b,c,1}, Min Su^{a,b,1}, Feng Gao^{a,b,1}, Wenjun Xie^{d,1}, Yang Zeng^{a,b,c,1}, De-lin Li^{a,b,c,1}, Xue-lei Liu^{a,b,c}, Hong Zhao^{a,b}, Li Qin^{a,b,c}, Fei Li^e, Qun Liu^f, Oliver B. Clarke^g, Sin Man Lam^a, Guang-hou Shui^a, Wayne A. Hendrickson^{g,h,2}, and Yu-hang Chen^{a,b,c,2}

Corresponding Authors: Yuhang Chen and Wayne A. Hendrickson

E-mail: yuhang.chen@genetics.ac.cn and wah2@cumc.columbia.edu

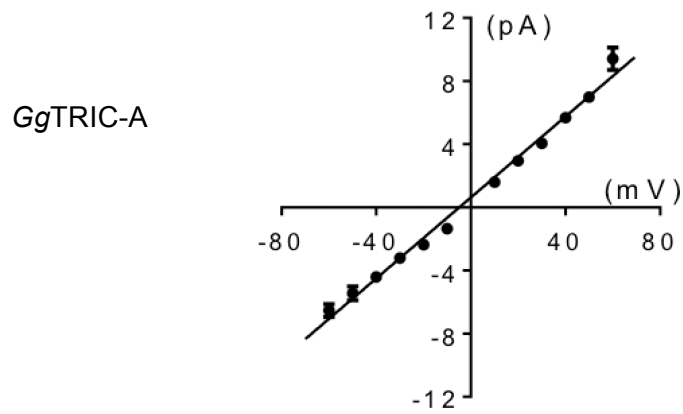
This PDF file includes:

Figs. S1 to S10

Supplementary text (includes SI reference citations)

Tables S1 to S3

A



B

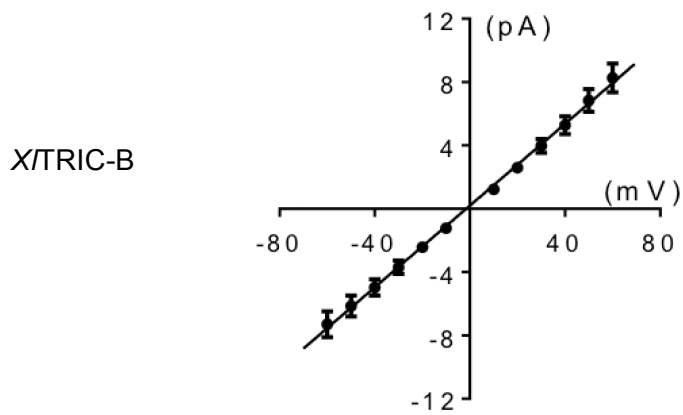


Figure S1. Current-Voltage relationship for vertebrate TRICs

(A) Current-Voltage relationship of GgTRIC-A channels. Solid fitting line represents a slope conductance of 128 ± 6 pS ($n=3$). (B) Current-voltage relationship of X/TRIC-B channels. Solid fitting line represents a slope conductance of 125 ± 13 pS ($n=3$).

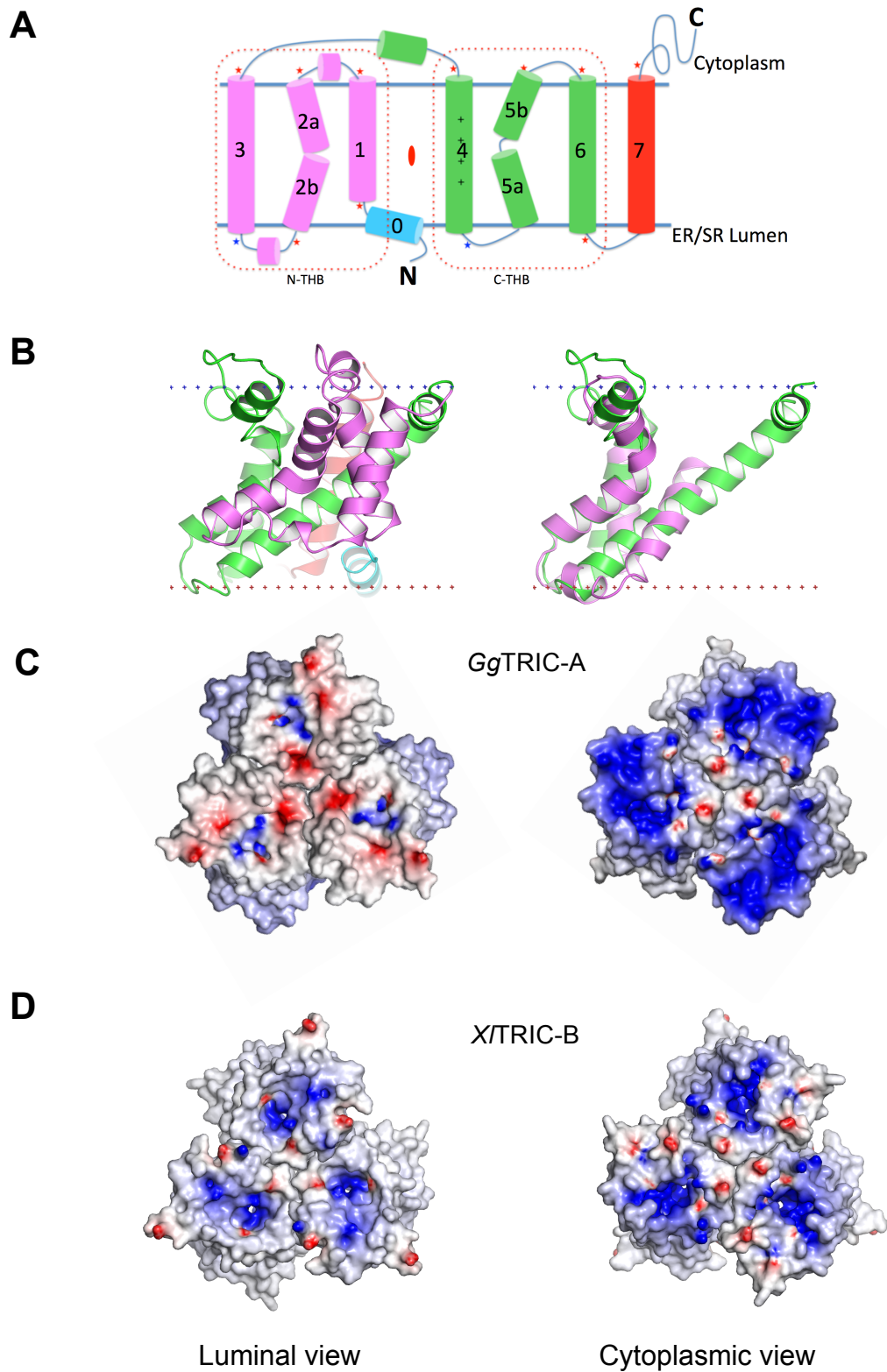


Figure S2. Structural characteristic of TRICs

(A) Membrane topology diagram for TRICs. TM₁₋₃ constitutes N-THB, and TM₄₋₆ constitutes C-THB, colored in purple and green, respectively. The additional TM₀ is in cyan and TM₇ is in red.

(B) Ribbon drawing of the *Gg*TRIC-A protomer (left panel), colored as in (A); The N-THB is superimposed on the C-THB (right panel). Membrane boundaries were calculated by using OPM server.

(C and D) Electrostatic potential at the solvent accessible contact surfaces for *Gg*TRIC-A (C) and *Xl*TRIC-B (D), as viewed from the luminal side, and from the cytoplasmic side. The contour level is at ± 7 kT/e; red for negative potential and blue for positive potential.

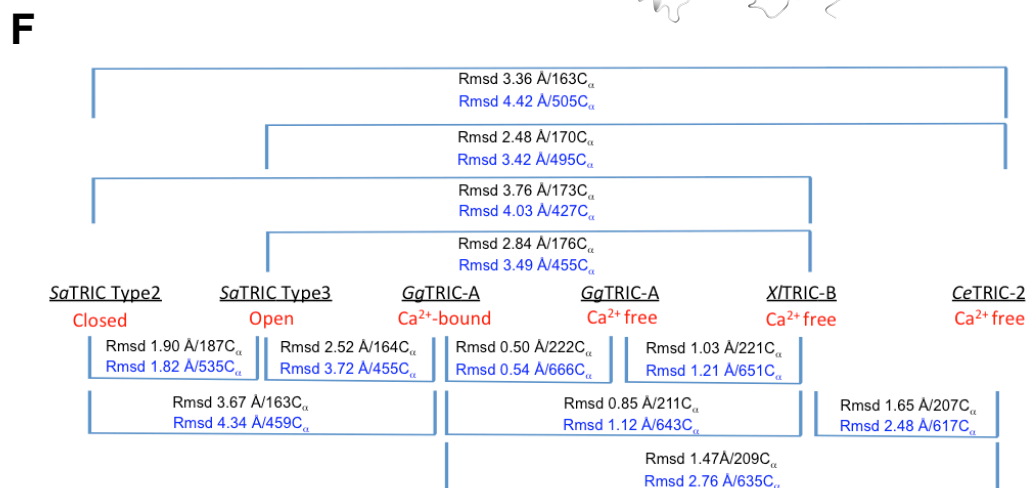
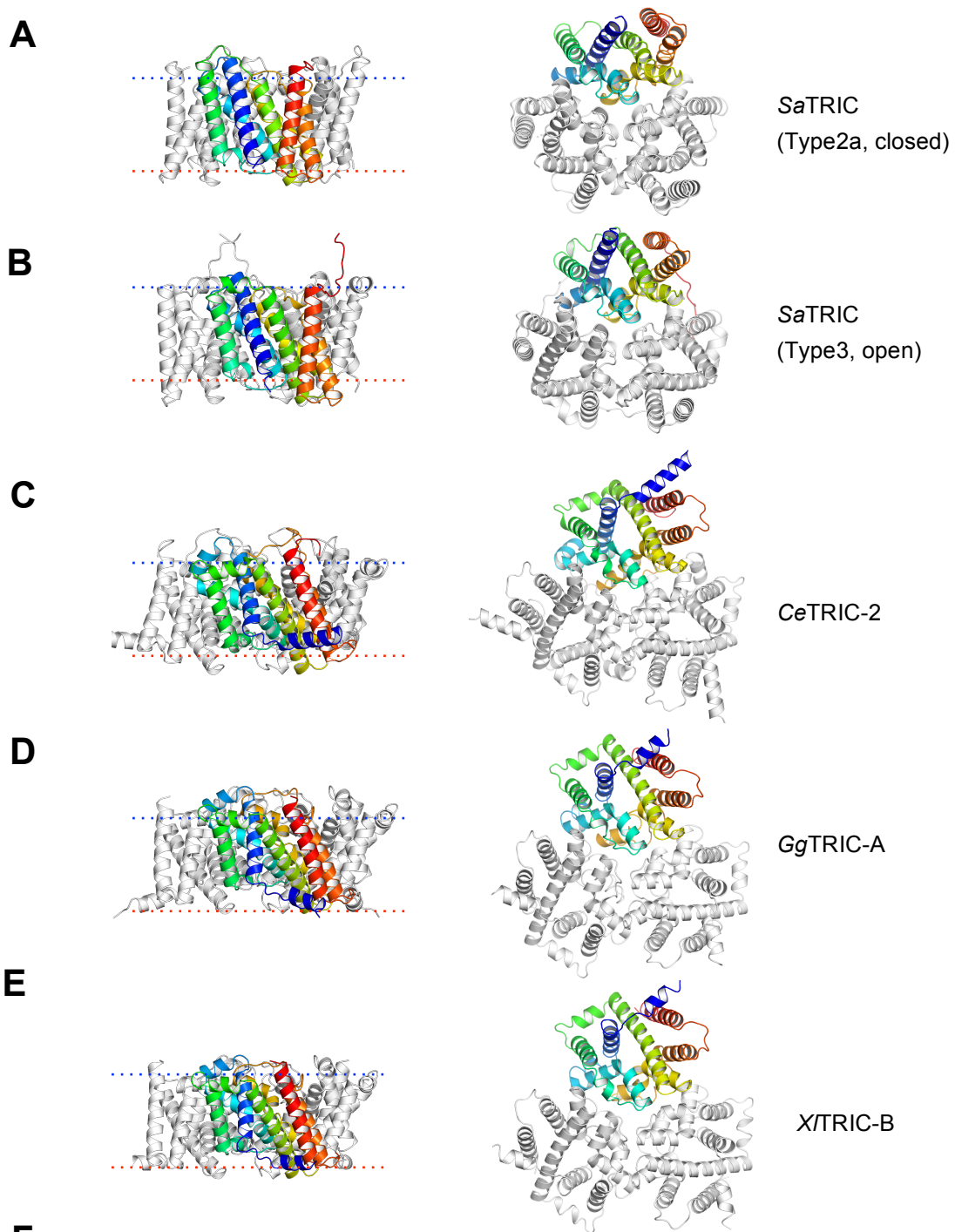
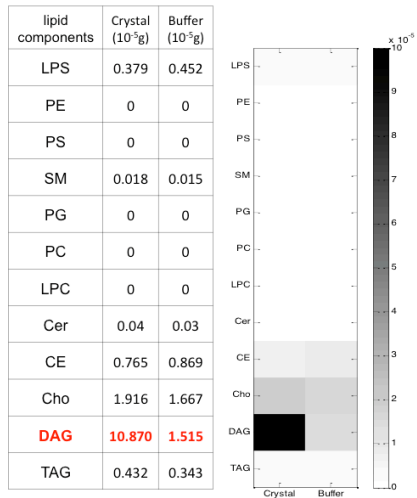


Figure S3. Structural comparison of TRICs

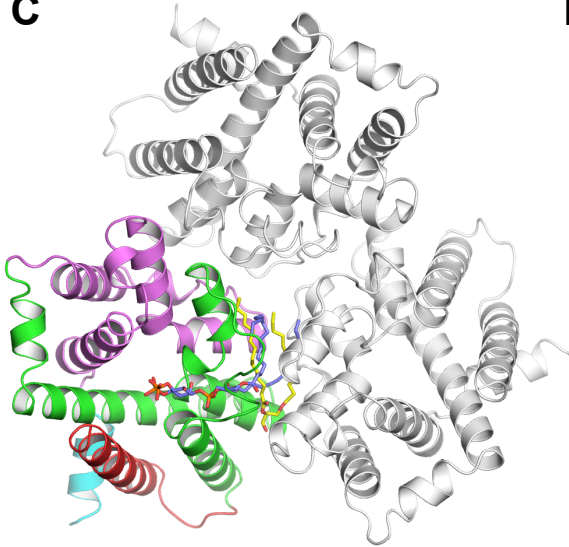
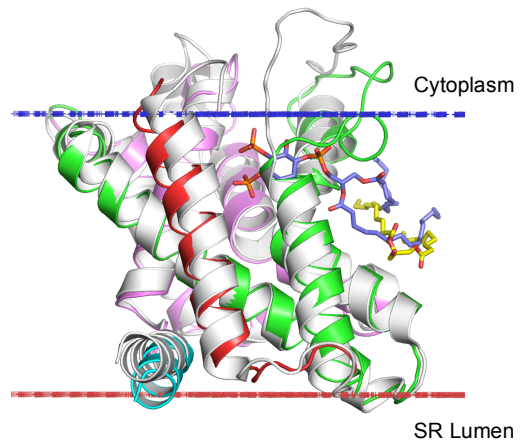
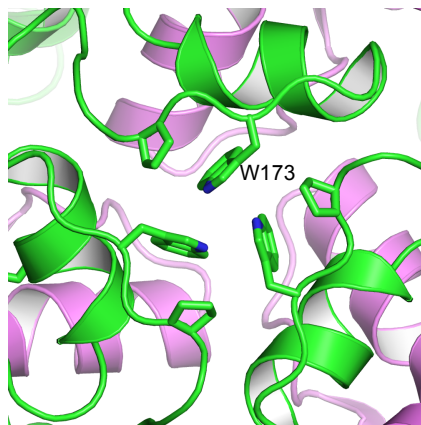
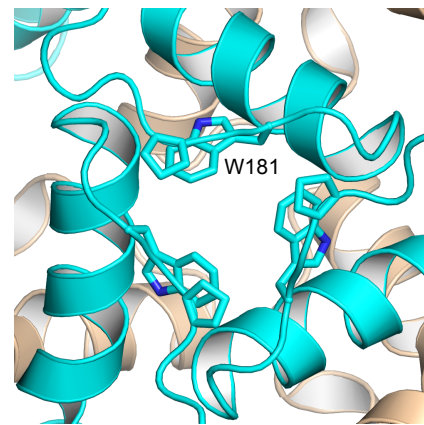
(A-E) Ribbon drawing of the trimer for various TRICs, as viewed from the membrane (left), and from the intracellular side (right). One protomer is colored spectrally from dark blue at its N-terminus to red at its C-terminus. From top to bottom: *Sa*TRIC (Type2a, closed), *Sa*TRIC (Type3, open), *Ce*TRIC-2, *Gg*TRIC-A and *X*/TRIC-B.

(F) Superimposition and statistics analyses for the protomer or trimer structure of various TRICs. R.m.s.d and superimposed C_α number are indicated.

A**B**

	Crystal (10 ⁻⁵ g)	Buffer (10 ⁻⁵ g)
DAG32:2(18:2/14:0)	0.013	0.009
DAG32:2(16:1/16:1)	0.038	0.023
DAG32:2(16:2/16:0)	0.015	0.014
DAG32:1(16:1/16:0)	0.044	0.016
DAG32:1(14:0/18:1)	0.014	0.006
DAG32:0(16:0/16:0)	4.110	0.222
DAG34:3(16:2/18:1)	0.089	0.075
DAG34:3(18:2/16:1)	0.029	0.166
DAG34:2(16:0/18:2)	0.036	0.025
DAG34:2(16:1/18:1)	0.107	0.021
DAG34:1(16:1/18:0)	0.040	0.036
DAG34:1(16:0/18:1)	0.179	0.018

	Crystal (10 ⁻⁵ g)	Buffer (10 ⁻⁵ g)
DAG34:0(16:0/18:0)	2.870	0.925
DAG36:4(18:2/18:2)	0.033	0.008
DAG36:3(18:2/18:1)	0.165	0.010
DAG36:2(18:1/18:1)	2.623	0.025
DAG36:2(18:2/18:0)	0.019	0.006
DAG36:1(18:1/18:0)	0.379	0.008
DAG40:6(18:0/22:6)	0.050	0.036
DAG40:5(18:0/22:5)	0.019	0.014

C**D****E****F****Figure S4. Comparison of lipid binding in TRICs**

(A) Lipidomics analysis of GgTRIC-A crystals. The lipid components in GgTRIC-A crystals are shown in the table and the heat-map (buffer as control). The enrichment of DAG is highlighted, as seen red in the table and black in the heat-map. LPS, lipopolysaccharides; PE, phosphatidylethanolamines; PS, phosphatidylserines; SM, sphingomyelins; PG, phosphatidylglycerols; PC, phosphatidylcholines; LPC, lysophosphatidylcholine; Cer, ceramide; CE, cholesteryl esters; Cho, cholesterol, DAG, diacylglycerol; TAG, triacylglycerol.

(B) Variants of DAGs are detected in the crystals. The most abundant DAG candidates are highlighted in red.

(C) Comparison of lipid binding mode in TRICs. Ribbon drawing of the GgTRIC-A trimer, with one protomer coloured as in Fig. S2d. The DAG molecules are shown as stick, and colored in yellow. Whereas the PIP₂ molecules observed in CeTRIC-2 was modeled into the GgTRIC-A through superimposed of TRICs structural model, and colored in blue.

(D) Superimposition of DAG-bound GgTRIC-A and PIP₂-bound CeTRIC-2. Ribbon drawings are shown for both GgTRIC-A and CeTRIC-2, with GgTRIC-A coloured as in (C), and CeTRIC-2 in grey. The DAG and PIP₂ molecules are shown, as in (C).

(E) Close-up views of the conformation of conserved W173 in the GgTRIC-A trimer.

(F) Close-up views of the conformation of conserved W181 in the CeTRIC-2 trimer.

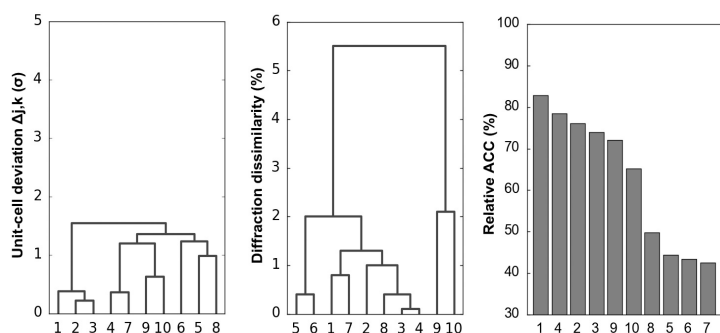
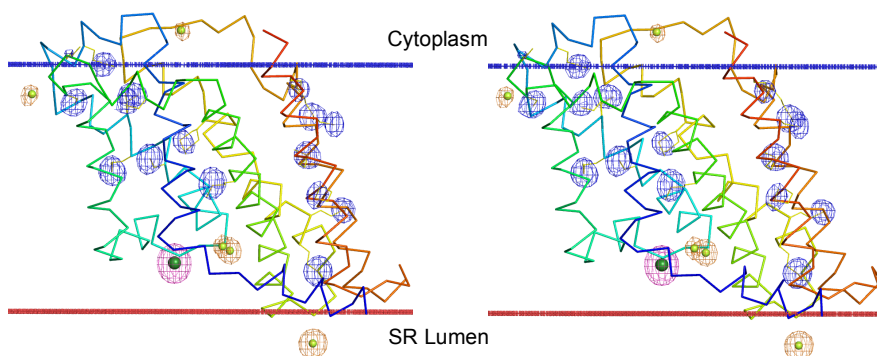
A**B**

Figure S5. Identification of anomalously scattering substructures in GgTRIC-A.

(A) Variations among crystals from 10 crystal data sets. Cluster analyses of unit cell variations (left); Cluster analyses of overall diffraction dissimilarity (center); Relative anomalous correlation coefficient (right).

(B) The stereo-view of Ca^{2+} -bound structure of GgTRIC-A, colored spectrally from dark blue at its N-terminus to red at its C-terminus. The bound anomalously scattering substructures for chloride and calcium are shown as spheres, and superimposed with anomalous density contours at 5.0σ . The bound Ca^{2+} ion is in dark green, and its anomalous density contours is in magenta. The bound chloride ions are in light green, and their anomalous density contours are in orange. Other anomalous density contours from the sulfur atoms are also shown in blue contours at 3.0σ .

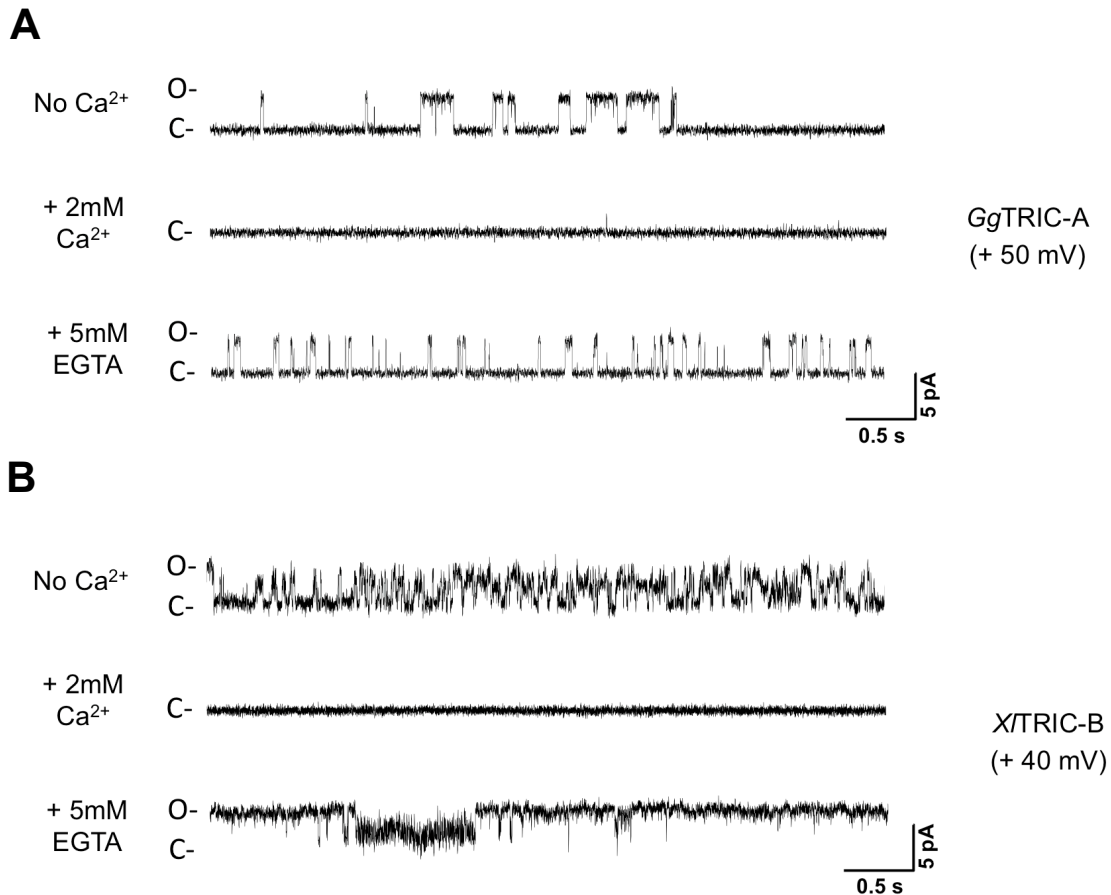
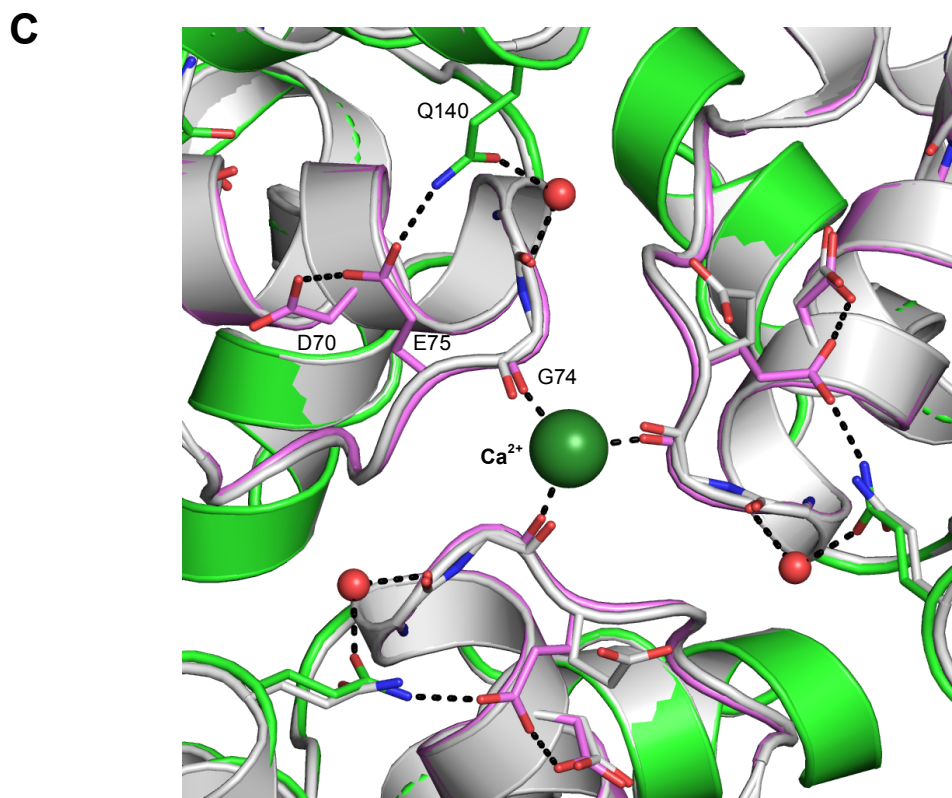
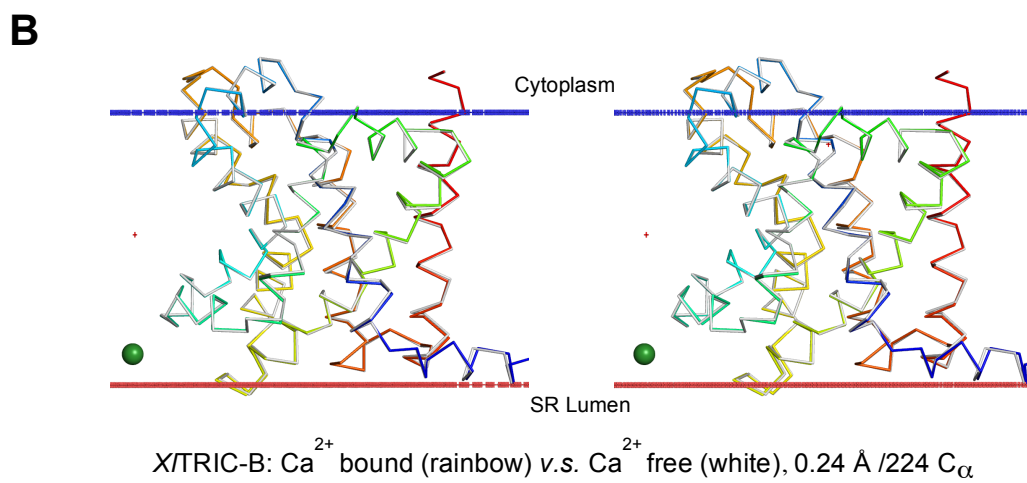
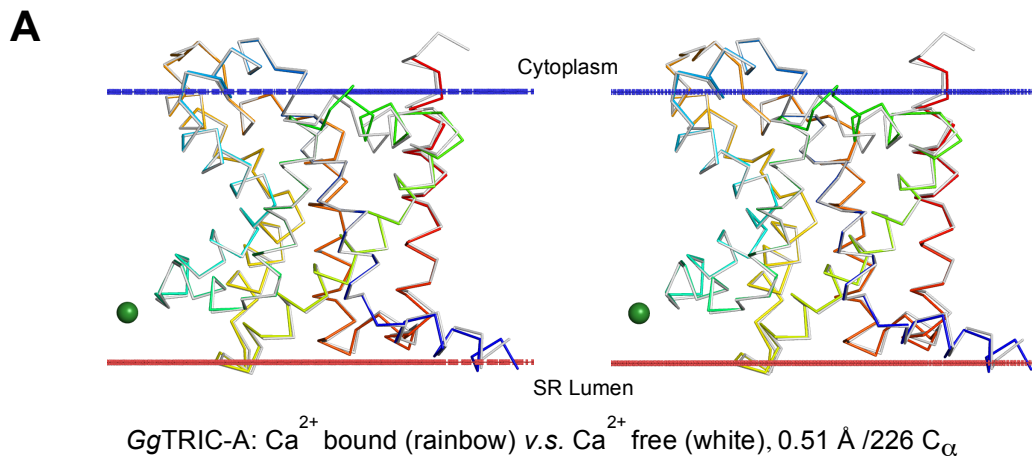


Figure S6. TRIC channel modulation by luminal Ca^{2+}

(A) GgTRIC-A channel modulation by luminal Ca^{2+} . Representative traces of single current recorded from planar lipid bilayers at +50 mV voltages (200 mM KCl in both *trans* and *cis* solutions), in the absence, presence of 2mM Ca^{2+} and addition of 5mM EGTA in the luminal side.

(B) X/TRIC-B channel modulation by luminal Ca^{2+} . Representative traces of single current recorded from planar lipid bilayers at +40 mV voltages (200 mM KCl in both *trans* and *cis* solutions), in the absence, presence of 2mM Ca^{2+} and addition of 5mM EGTA at the luminal side.

Orientation established as the asymmetrically charged TRIC protein is fused to the lipid bilayer held in an applied *cis*-bilayer potential.



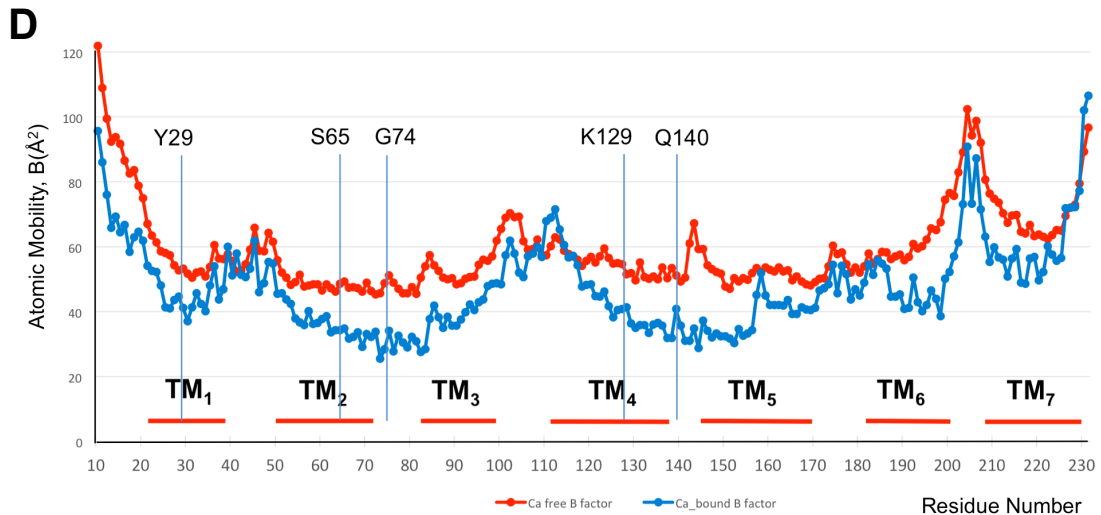


Figure S7. Structural comparison of TRICs: Ca²⁺-bound and Ca²⁺-free.

(A) The stereo-view of Ca²⁺-bound structure (rainbow), superimposed with Ca²⁺-free structure (white) of GgTRIC-A. The r.m.s.d is 0.51 Å for the 226 superimposed C_α.

(B) The stereo-view of Ca²⁺-bound structure (rainbow), superimposed with Ca²⁺-free structure (white) of X/TRIC-B. The r.m.s.d is 0.24 Å for 224 superimposed C_α.

(C) A close-up view of the superimposition of GgTRIC-A, Ca²⁺-bound structure vs. Ca²⁺-free structure, as viewed from luminal side. The structures are colored as in Fig. 5D.

(D) Atomic mobility profiles comparing Ca²⁺-bound (blue) and Ca²⁺-free (red) structures of GgTRIC-A. B-factors of C_α residues are plotted as a function of residue number. Transmembrane helix spans are marked by red bars and residues involved in TM₂-TM₄ contacts and the positions of K129 gating contacts are indicated.

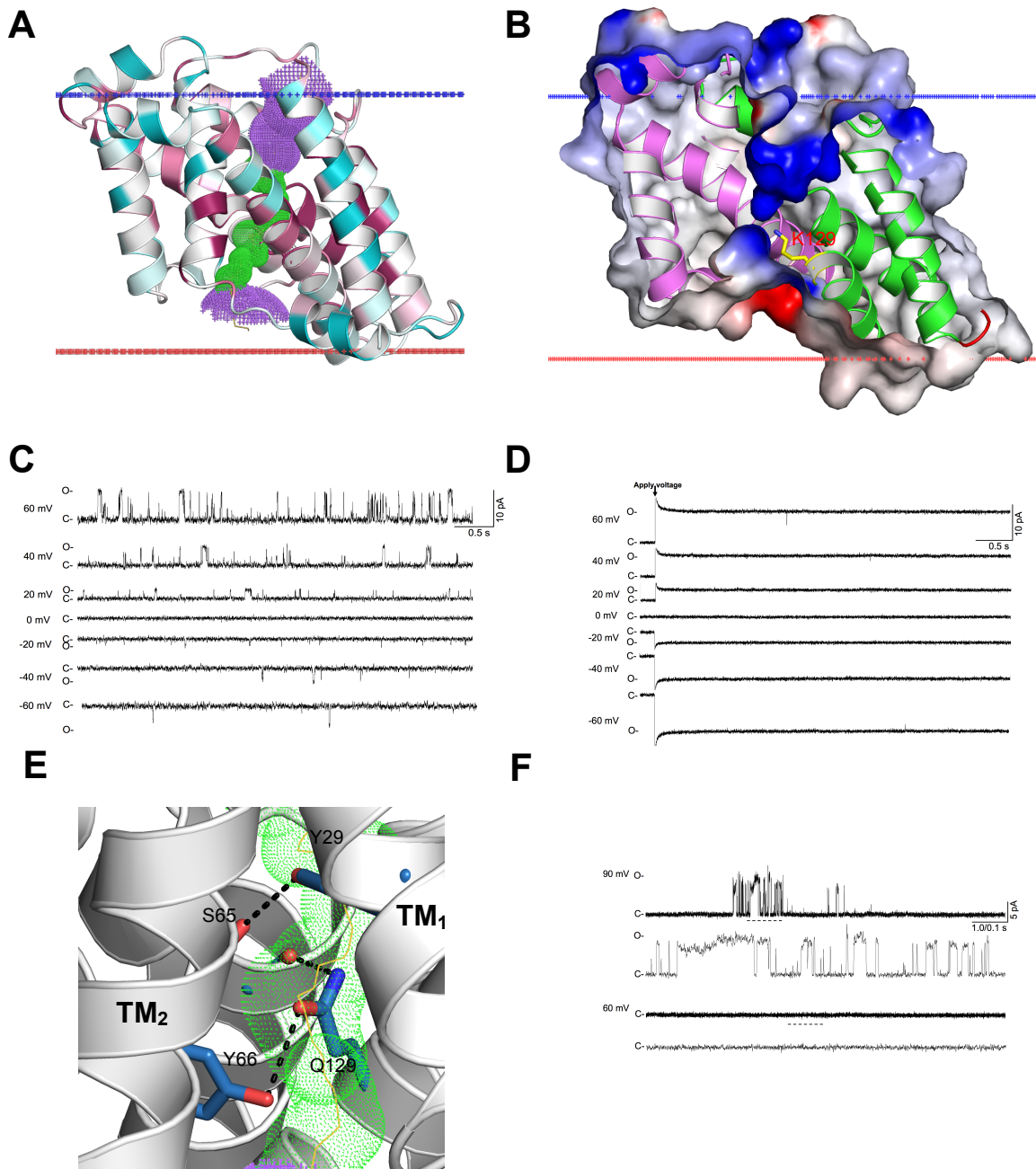


Figure S8. Structural feature of TRIC pore

(A) The pore lining surface for *Gg*TRIC-A K129A as computed by the program HOLE is drawn into a ribbon model of the protomer structure of *Gg*TRIC-A, colored by sequence conservation, as in Fig. 1B.

(B) Cross-section through the *Gg*TRIC-A reveal the electropositive feature of the channel pore.

(C and D) Representative traces of GgTRIC-A currents, wild type (C) and K129A mutant (D), recorded from planar lipid bilayers at different voltages (200 mM KCl in *both trans and cis* solutions).

(E) Close-up view of the conserved K129Q plug and its hydrogen bonded interaction with Y66 and K155. The pore lining surface for GgTRIC-A K129A is superimposed into the ribbon model of GgTRIC-A K129Q mutant. Q129 protrudes into the pore and is stabilized by hydrogen bonds with Y66 and K155, thus blocking the channel.

(F) Representative current traces of GgTRIC-A K129Q mutant, recorded from planar lipid bilayers at +60mV and +90mV voltages (200 mM KCl in both *trans* and *cis* solutions).

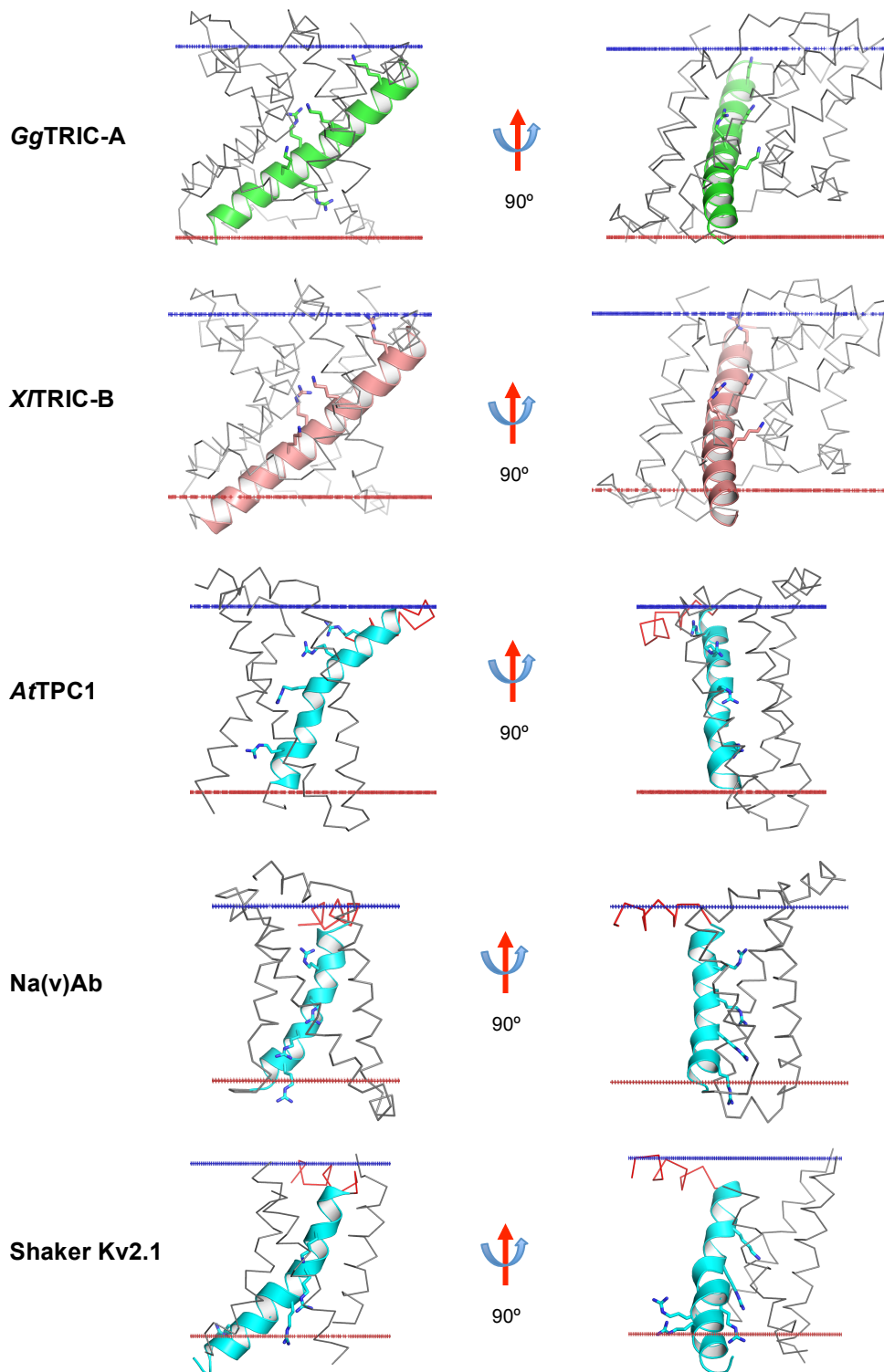
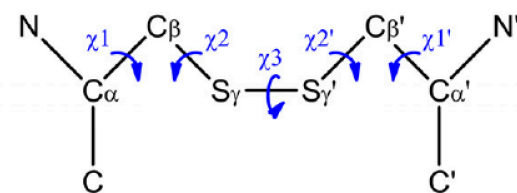


Figure S9. Comparison of voltage sensor element of TRICs with various voltage-regulated channels. From top to bottom: Chicken GgTRIC-A, Xenopus X/TRIC-B, Arabidopsis AfTPC1 (PDB ID: 5dqq), Arcobacter Nav_{Ab} (PDB ID: 3rvy) and Rattus Kv1.2 (PDB ID: 2a79). The highly conserved positive-charge residues are shown as sticks. The membrane boundary was calculated by the OPM server.



Cys Pair	Bond Dist. (Å)		Torsion Angle (°)					Bond Angle (°)				
	S-S	Cα-Cα	χ1	χ2	χ3	χ2'	χ1'	Cα-Cβ-Sγ	Cβ-Sγ-Sγ'	Sγ-Sγ'-Cβ'	Sγ'-Cβ'-Cα'	
25-125	2.04	6.56	56.7	-101.9	169.3	82.2	-83.3	114.2	106.9	108.3	116	
127-217	2.02	5.97	45	148.5	114.9	-78.9	-56.7	115.7	105.2	109.2	117.8	
137-151	2.01	6.60	179.7	-166.2	-102.6	-169.6	-64.3	105.2	107	97.2	116.9	
Ideal value	LH	2.02	5.8	±60/±180		-80		±60/±180	114	105	105	114
	RH	2.02	5.4	±60/±180		100		±60/±180	114	105	105	114

LH: Left-handed disulphide bridge; RH: Right-handed disulphide bridge.

Figure S10. Geometry analysis for engineered GgTRIC-A-disulfide bonds

The conformations of disulfide bonds in proteins are defined by dispositions of six atoms, $C\alpha-C\beta-S\gamma-S\gamma'-C\beta'-C\alpha'$, linking the two cysteine residues. Geometry minimization in PHENIX has been applied for the mutated cysteine pairs (Cys25/Cys125, Cys127/Cys217, Cys137/Cys151) as modeled into the structure. The table shows a detailed analysis on the bond distances, bond angles and torsion angles for each mutated cysteine pair. Ideal values for bond distance/angle and torsion angle were shown for both the left-handed disulfide bridge and the right-handed disulfide bridge (1). The “outliner values” from a Molprobit check are highlighted in red.

Supplemental Materials and Methods

Bioinformatics analysis of TRIC proteins

Sequences related to the eukaryotic TRIC-A or TRIC-B were analysed comprehensively by PSI-BLAST, using similar procedure (2). Searches at $E < 10^{-3}$ starting from five disparate homologs each identified a common pool of about 800 protein sequences, which when pooled were used for further clean-up and sub-classification into families and subfamilies. Details of these analyses are reported in footnotes to Table S1.

Cloning and expression

Eight pairs of vertebrate TRIC-A and TRIC-B, including human, mouse, rat, chicken, bovine, rabbit, frog and zebra fish, were selected for gene synthesis with codon optimization and cloned into a modified pREP1 vector with a FLAG and deca-histidine tag at the C-terminus (cleavable by TEV protease) for expression in the yeast *S. Pombe*. The resulting constructs were transformed into a Leucine auxotroph *S.pombe* strain by lithium acetate method, and standard media for fission yeast were used (3). The transformants were negatively selected by plating on the EMM plates without leucine, but 15 μ M thiamine inhibits the promoter. Point mutations of cysteine to serine have been introduced to improve protein behaviour by avoiding the possible disulphide bond formation. The point mutation of C245S had been selected for GgTRIC-A and has better behaviour and passed for further structural studies.

Scaled-up production and purification

In brief, for preparation of the seed, the transformed yeast *S. pombe* cells was inoculate in ~ 150 ml EMM culture medium, supplemented with 25 μ M thiamine for ~ 36 hours at 30 °C and 200 rpm. The protein expression was initiated by removal of the thiamine in the culture media. For protein expression and scale up, the cells were spun down, and washed with sterile ddH₂O twice before further inoculation to large culture of ~ 0.5-1.0 liter. The cells were first grown at 30 °C and 200 rpm for ~12 hours, and supplemented with equal volume of fresh media and continue to grow for another 12 hours. The cells were harvested by centrifugation and stored at -80°C before use.

For preparation of selenomethionyl (Se-Met) GgTRIC-A, the plasmid was transformed into a leucine and methionine double auxotroph *S.pombe* strain. The proteins were expressed in a similar way as the native protein by adding 25-50 mg/L Se-Met in the defined EMM minimal media.

Cells were re-suspended in a buffer containing 50 mM Tris-HCl (pH 8.0) and 200 mM NaCl and lysed using a French Press with four passes at ~15-20,000 psi. Cell debris was removed by centrifugation at 10,000g for 20min, and the membrane fraction was isolated from that supernatant by ultra-centrifugation at 150,000g for 1 hour. The membrane fraction was homogenized in a solubilization buffer containing: 50 mM Tris (pH 8.0), 200 mM NaCl, and, 2.5% Glycerol, and incubated with final concentration of 1.5 % (w/v) n-dodecyl- β -D-maltopyranoside (DDM, Anatrace, Inc) by gentle stirring for 1 hour at 4°C. The non-dissolved matter was removed by ultracentrifugation at 150,000g for 30 min, and the supernatant was loaded to a 5ml HiTrap Ni²⁺-NTA affinity column (GE Healthcare), pre-equilibrated with the same solubilization buffer supplemented with 0.05% DDM. After 20 columns volume buffer wash, the protein was eluted with 350mM imidazole in the solubilization buffer. The Flag and 10-His tags were removed by adding super TEV (4)(tobacco etch virus protease) at 1:1000 mass ratio and incubating at 4°C overnight. Tag removal was confirmed by SDS-PAGE, and the resulting sample was concentrated to around 10mg/ml. Preparative size exclusion chromatography was carried out on a Superdex-200 10/300 GL (GE Healthcare) column for further purification, removal of TEV protease and the cleaved tag, and for buffer and detergent exchange. The gel-filtration buffer contained 20 mM Hepe-Na (pH 5.4 or 7.5), 200 mM NaCl, 1% Glycerol, and 2xCMC of detergent. In the case of GgTRIC-A and X/TRIC-B, the proteins were well behaved and stable in nearly all tested detergents, including DDM, DM, OM, NGOG, OG and LDAO.

Protein crystallization and data measurement

Purified GgTRIC-A and X/TRIC protein in a series of detergents, including DDM, DM, OM and NGOG, were concentrated to ~10mg/ml for initial crystal trials manually via the sparse-matrix screening method with commercial screens from Hampton research,

Emerald Biosystems and Molecular Dimension. The crystals were grown by mixing protein and solution via 1:1 ratio at 4 °C using sitting drop vapour diffusion methods (table S2).

Native and Se-Met SAD data sets were collected at variable wavelength at multiple beam-lines, including BL17U and BL19U at Shanghai Synchrotron Radiation Facility (SSRF) and at 24IDC at Advanced Photon Source (APS), and processed with the software XDS(5).

Structural determination

When solubilized in detergent OGNG micelle, the *Gg*TRIC-A was crystallized in the presence of 100mM CaCl₂ in space group P6₃22, with a=b=127.45 Å and c= 102.12 Å. The structure was solved by selenomethionyl (Se-Met) SAD phasing(6) with data collected at 0.97853 Å, ultimately at 2.2 Å resolution, and then refined at 1.8 Å resolution to R_{work}/R_{free} values of 18.2% / 20.6%, containing ordered residues 8-231, 1 Ca²⁺ ion, 6 Br⁻ ion and 89 water molecules(7, 8). C-terminal residues 232-296 are not visible in the structure, due to its intrinsic flexibility. The Ca²⁺-free *Gg*TRIC-A structure was determined to 2.2 Å resolution in a cubic lattice (F4₁32, a = 268.2 Å) by molecular replacement, with R_{work}/R_{free} values of 25.5%/26.9%, and ordered residues 10-234. Other structures of *Gg*TRIC-A from various conditions or mutants are solved by molecular replacement. The *X*TRIC-B was crystallized in multiple lattices and the structure was first solved to 3.8 Å in lattice of F432, and later to 3.1 Å in lattice of P4₁22 in the absence of Ca²⁺ by molecular replacement. The final model contained residues 4-227, with R_{work}/R_{free} values of 29.4%/30.7%. The Ca²⁺-bound *X*TRIC-B was determined to 3.3 Å in lattice of F432, with R_{work}/R_{free} values of 30.8%/32.1%, containing residues 4-227 and 1 Ca²⁺ ion (For details, see table S2, S3). Structure validation was performed with Molprobity(9). Figures were prepared in PyMOL (<http://www.pymol.org>).

f” refinement for ion identification

To further identify ion bindings within the channel protein, we also solved high-resolution structure by using data collected at low energy wavelength (1.7712 Å),

and merged from multiple isomorphous crystals (Fig. S5A). The structure was refined at 2.0 Å resolution to $R_{\text{work}}/R_{\text{free}}$ values of 18.4% / 20.2%, containing ordered residues 8-231, 1 Ca^{2+} ion, 5 Cl^- ions, 101 water molecules, and 1 DAG molecules. The identification of ions (Ca^{2+} and Cl^-) binding was based on the anomalous Fourier maps as well as the geometry and coordination with the surrounding residues and water molecules, and further confirmed by the refinement of f'' of the corresponding element(7, 10, 11). In final refined structure at 2.0 Å resolution, the selected ten fitted f'' for Sulfur (S_{protein}) have an average value of 0.77 ± 0.06 e, which is within 3σ of the theoretical value of 0.699 e, indicating the quality of refinement procedure is reliable. Besides the well-ordered Sulfur sites in the protein, we also identified five well-resolved Cl^- sites associated with the protein, with five fitted $f''(\text{Cl}^-)$ average value 0.90 ± 0.27 e (theoretical value 0.883 e); and one strong peak for Ca^{2+} on the luminal side along the three fold axis of the trimeric channel, with the fitted $f''(\text{Ca}^{2+})$ value of 1.82 e (theoretical value 1.598 e). All the anomalous sites are consistent with the Bijvoet-different map.

Lipidomics analysis of GgTRIC-A crystals

Crystals for GgTRIC-A were harvested and re-dissolved at the buffer containing 20mM HEPES-Na, pH 7.5, 200mM NaCl, 1% Glycerol, 3mM NGOG, which make the final concentration at 2mg/ml. Specific volumes of protein mixtures (~ 75 μL) were aliquoted for lipid extraction to achieve a final protein amount at 0.15 mg. Equal volume of blank buffer was extracted to serve as a negative control. The protein solution were extracted using a modified version of the Bligh and Dyer's protocol, and lipid extracts were analysed on an Agilent HPLC 1260 system coupled with Sciex QTRAP 5500 as described previously(12).

Electrophysiology

Purified proteins of GgTRIC-A and XTRIC-B (wild type and mutants), at final concentration between 1 μg to 5 $\mu\text{g ml}^{-1}$, were fused into planar lipid bilayers formed by painting a lipid mixture of phosphatidylethanolamine (DOPE) and phosphatidylcholine (DOPC) (Avanti Polar Lipids) in a 3:1 ratio in decane across a

200- μ m hole in a polystyrene partition separating the internal and external solutions in poly-sulfonate cups (Warner Instruments). The *cis*-chamber (1.0 ml), representing the intra-SR (luminal) compartment, was connected to the head stage input of a bilayer voltage clamp amplifier. The *trans*-chamber (1.0 ml), representing the cytoplasmic compartment, was held at virtual ground. Solutions in both *trans*- and *cis*-chamber were as follows (in mM): 200 KCl, and 10 HEPES (pH 7.4). Purified TRIC proteins were added to the *trans*-chamber with a pre-applied +30mV at the *cis*-chamber. The TRIC proteins will fuse to the lipid bilayer with a preferred direction, with their electro-negative luminal side of the protein facing the *cis*-chamber, and the electro-positive one facing *trans*-chamber. Currents were recorded every minute after application of the voltage to the *cis*-side. Single-channel currents were recorded using a BC-535 Bilayer Clamp amplifier (Warner Instruments, LLC, CT), filtered at 1kHz using a Low-Pass 8-pole Bessel Filter (Warner Instruments, LLC, CT), and digitized at 4 kHz. All experiments were performed at room temperature (23 ± 2 °C). pH for the solution was adjusted with choline. Single-channel P_o was determined over 1 minute of continuous recording using the method of 50% threshold analysis. The recordings were analysed by using Clampfit 10.1 (Molecular Devices) and Prism (ver.5.0, GraphPad).

Cysteine crosslinking.

For CuP-promoted oxidation, purified proteins (~0.2 mg/ml) incubated for 30 min at ~25°C with 500 μ M CuSO₄ and 500 μ M 1,10-phenanthroline (Sigma, St Louis, MO, USA). The reaction was quenched by 10 μ M N-ethylmaleimide (13).

REFERENCES

1. Petersen MT, Jonson PH, & Petersen SB (1999) Amino acid neighbours and detailed conformational analysis of cysteines in proteins. *Protein engineering* **12**:535-548.
2. Altschul SF, *et al.* (1997) Gapped BLAST and PSI-BLAST: a new generation of protein database search programs. *Nucleic Acids Res* **25**:3389-3402.
3. Dong QH, *et al.* (2016) Ccp1 Homodimer Mediates Chromatin Integrity by Antagonizing CENP-A Loading. *Mol cell* **64**:79-91.

4. Kapust RB, *et al.* (2001) Tobacco etch virus protease: mechanism of autolysis and rational design of stable mutants with wild-type catalytic proficiency. *Protein engineering* **14**:993-1000.
5. Kabsch W (2010) XDS. *Acta Cryst D* **66**:125-132.
6. Pape T & Schneider TR (2004) HKL2MAP: a graphical user interface for macromolecular phasing with SHELX programs. *J Applied Cryst* **37**:843-844.
7. Adams PD, *et al.* (2010) PHENIX: a comprehensive Python-based system for macromolecular structure solution. *Acta Cryst D* **66**:213-221.
8. Emsley P, Lohkamp B, Scott WG, & Cowtan K (2010) Features and development of Coot. *Acta Cryst D* **66**:486-501.
9. Chen VB, *et al.* (2010) MolProbity: all-atom structure validation for macromolecular crystallography. *Acta Cryst D* **66**:12-21.
10. Liu Q, *et al.* (2012) Structures from Anomalous Diffraction of Native Biological Macromolecules. *Science* **336**:1033-1037.
11. Liu Q, Liu QL, & Hendrickson WA (2013) Robust structural analysis of native biological macromolecules from multi-crystal anomalous diffraction data. *Acta Cryst D* **69**:1314-1332.
12. Gong H, *et al.* (2018) An electron transfer path connects subunits of a mycobacterial respiratory supercomplex. *Science* **362**:aatt8923, DOI: 10.1126/science.aat8923
13. Mancia F, Assur Z, Herman AG, Siegel R, & Hendrickson WA (2008) Ligand sensitivity in dimeric associations of the serotonin 5HT2c receptor. *EMBO Rep* **9**:363-369.

Table S1. PSI-BLAST analysis of eukaryotic TRIC-related proteins

Family	Expansion sequence ^a	GenBank ID	$-\log(E_{\text{cut}})$	Initial	Final	Sequence identity < 100%
Eukaryotic TRICs	<i>HsTRIC-A</i>	74733603	3	425	421	419
	<i>HsTRIC-B</i>	8922461				
	<i>DmTRIC</i>	18859841				
	<i>CeTRIC_1</i>	290457497				
	<i>CeTRIC_2</i>	34556095				
Vertebrate TRICs	<i>HsTRIC-A</i> <i>HsTRIC-B</i>	74733603 8922461	60	254	250	249
Invertebrate TRICs	<i>DmTRIC</i> <i>CeTRIC_1</i> <i>CeTRIC_2</i>	18859841 290457497 34556095	60	138	138	137
Other				33	33	33
Total				425	421	419
TRIC-As	<i>HsTRIC-A</i>	74733603	90	138 ^b	118	117
TRIC-Bs	<i>HsTRIC-B</i>	8922461	90	128 ^b	126	126
Other				6	6	6
Total				254	250	249

a. The alternative expansion sequences used to generate a common pool for defining the eukaryotic TRICs superfamily, the vertebrate TRICs and invertebrate TRICs families.

b. The TRIC-A and TRIC-B subfamilies expansions cover most of the vertebrate TRIC family, but there is a small portion of 18 overlapped sequences, which were further assigned into TRIC-B subfamily based on some common features.

c. Procedures for the PSI-BLAST analysis of the TRIC superfamily:

PSI-BLAST construction of common pool. NCBI PSI-BLAST was run against the non-redundant (nr) database (GenBank CDS translations + PDB entries + SwissProt entries + PIR entries + PDF entries + PRF entries) starting from three different defining expansion sequences based on selected diverse apparent homologs (GenBank IDs 74733603, 8922461, 18859841, 290457497 and 34556095) at E-value cutoff (E_{cut}) of 10^{-3} . Each sequence reached convergence at the 2th or 3th PSI-BLAST run, having generated 810~830 sequences. Some 800 sequences were in common, and this pool of common sequences was reduced to 600 after removal of some partial or non-relevant sequences: i) removal of sequences >500 residues, ii) removal of sequences <240 residues, iii) removal of sequences not having a starting Met, and iii) removal of sequences containing an X. Further purification was performed based on the sequence alignment. In particular, CLUSTAL W was used to perform multiple sequence alignment, and sequences obviously lacking some TM helix were removed. This resulted in the set

of 425 sequences that we have used here to define the family organization.

PSI-BLAST rounds of sub-classification. The 425 identified sequences were used to establish a local PSI-BLAST database into which various sequences were expanded at various E_{cut} levels. We found that at $E_{cut} = 10^{-60}$ there was two distinct groups, the vertebrate TRIC and invertebrate TRIC families, plus a number of others. Within the vertebrate TRIC, subfamilies of TRIC-A and TRIC-B were established at the level of $E_{cut} = 10^{-90}$. A final check for redundancy was then made to achieve the set of 'Sequence identity < 100%'.

d. The representative sequences were computed by the program COBALT. The selected sequence, with their abbreviation and UniProtKB or NCBI entry name, are listed as below:

Vertebrate TRIC-As:

Mm - Mouse *Mm*TRIC-A (Q3TMP8); Oc - Rabbit *Oc*TRIC-A (A5A6S6); Bt - Bovine *Bt*TRIC-A (A4FV75); Hs - Human *Hs*TRIC-A (Q9H6F2); Gg - Chicken *Gg*TRIC-A (Q5ZK43); Am - Alligator *Am*TRIC-A (A0A151NZ50); XI - Xenopus *Xt*TRIC-A (Q7ZY07); Dr - Zebrafish *Dr*TRIC-A (Q6P2T0).

Vertebrate TRIC-Bs:

Mm - Mouse *Mm*TRIC-B (Q9DAV9); Oc - Rabbit *Oc*TRIC-B (G1SPQ1); Bt - Bovine *Bt*TRIC-B (Q0VC58); Hs - Human *Hs*TRIC-B (Q9NVV0); Gg - Chicken *Gg*TRIC-B (R4GGD2); Am - Alligator *Am*TRIC-B (A0A151NEF0); XI - Xenopus *Xt*TRIC-B (Q6GN30); Dr - Zebrafish *Dr*TRIC-B (Q7ZVP8).

Invertebrate TRICs:

Dm - Drosophila *Dm*TRIC (18859841); Px - *Px*TRIC (I4DN83); Apis - *Am*TRIC (A0A087ZY47); Rp - *Rp*TRIC (R4WIN7); Lp1 - *Lp*TRIC-1(XP_013787888); Lp2 - *Lp*TRIC-2 (XP_013791185); Tp - *Tp*TRIC (A0A0V1DZZ3); Ce1 - *Ce*TRIC-1(Q9NA75); Ce2 - *Ce*TRIC-2 (Q9NA73).

Green Alga TRICs:

OI - *Ot*TRIC (A4RWC2); Mp - *Mp*TRIC(C1N4G0).

Archaeal TRICs:

Ss - *Ss*TRIC (Q981D4); Sa - *Sa*TRIC (M1IV35).

Bacterial TRICs:

Va - *Va*TRIC (C2HUB6); Bf - *Bf*TRIC (Q5LE06); Cp - *Cp*TRIC (Q47UY7); Ec - *Ec*TRIC (P0AFP0); Ac - *Ac*TRIC (Q9R9S0).

Table S2. Summary table for crystallization and structural analysis of TRICs

	Table S2a GgTRIC-A Wild Type				Table S2b GgTRIC-A Mutant	
Dataset_name	WT_Se	WT_Ca12k	WT_Ca7k	WT_Ca_free	K129A	K129Q
Protein Type	SeMet	Native	Native	Native	Native	Native
Protein Solution	Hepe-Na 20mM pH5.4, NaCl 200mM, NG311 3mM	Hepe-Na 20mM pH5.4, KBr 200mM, NG311 3mM	Hepe-Na 20mM pH5.4, NaCl 200mM, NG311 3mM	Hepe-Na 20mM pH5.4, NaCl 200mM, NG311 3mM	Hepe-Na 20mM pH5.4, NaCl 200mM, NG311 3mM	Hepe-Na 20mM pH5.4, NaCl 200mM, NG311 3mM
Wavelength	0.9785 Å	0.9785 Å	1.7712 Å	0.9785 Å	0.9792 Å	0.9792 Å
Space group	P6 ₃ 22	P6 ₃ 22	P6 ₃ 22	F4 ₁ 32	P6 ₃ 22	P6 ₃ 22
Resolution	2.2 Å	1.80 Å	2.0 Å (from 10 crystals)	2.2 Å	2.3 Å	2.4 Å
Solution for crystallization	PEGMME2000 11%, CaCl ₂ 100mM, Tris-HCl pH 6.5 100mM, 10mM Betaine, 8%Glycerol / 3% MPD,	PEGMME2000 9%, CaCl ₂ 100mM, Tris-HCl pH 6.5 100mM, 10mM EDTA, 6%Glycerol,	PEGMME2000 11%, CaCl ₂ 100mM, Tris-HCl pH 6.5 100mM, 10mM Betaine, 8%Glycerol,	1.6 M NaH ₂ PO ₄ , 0.4 M K ₂ HPO ₄ , phosphate-citrate pH 4.2 100mM,	PEGMME2000 11%, CaCl ₂ 100mM, Tris-HCl pH 6.5 100mM, 10mM EDTA, 8%Glycerol	PEGMME2000 11%, CaCl ₂ 100mM, Tris-HCl pH 6.5 100mM, 10mM Betaine, 8%Glycerol,
Method for crystallization	Detergent micelle	Detergent micelle	Detergent micelle	Detergent micelle	Detergent micelle	Detergent micelle
Molecular Construct	1-298, C245S, Se-Met	1-298, C245S, Native	1-298, C245S, Native	1-298, C245S, Native	1-298, C245S, K129A Native	1-298, C245S, K129Q Native
Ion binding along 3-fold axis, bound to G74	1 Ca ²⁺	1 Ca ²⁺	1 Ca ²⁺	None	1 Ca ²⁺	1 Ca ²⁺
Beamline Facility	SSRF 19U1	SSRF 19U1	APS_24IDC	SSRF 19U1	SSRF 19U1	SSRF 19U1

Table S2c XTRIC-B Wild Type				
Dataset_name	WT_Ca_free1	WT_Ca_free2	WT_Ca_free3	WT_Ca
Protein Type	Native	Native	Native	Native
Protein Solution	Hepe-Na 20mM pH7.4, NaCl 200mM, NG311 3mM	Hepe-Na 20mM pH5.4, NaCl 200mM, NG311 3mM	Hepe-Na 20mM pH5.4, NaCl 200mM, NG311 3mM	Hepe-Na 20mM pH5.4, NaCl 200mM, NG311 3mM
Wavelength	1.7712 Å	1.7712 Å	0.9778 Å	1.7712 Å
Space group	F432	P32	P4 ₂ 2 ₁ 2	F432
Resolution	3.70 Å (merge 2 dataset from 1 crystal)	3.80Å (merge 2 dataset from 2 crystals)	3.10 Å (1 dataset from 1 crystal)	3.30 Å (1 dataset from 1 crystal)
Solution for crystallization	PEG 400 22%, MgCl ₂ , 50mM Glycine pH 9.0 100mM	PEG 4000 7.7%, KNO ₃ 20mM, K-Citrate pH 6.5 30mM,	PEG 400 22%, MgCl ₂ , 50mM Glycine pH 9.0 100mM	PEG 350 MME 26%, CaCl ₂ , 200mM MES pH 6.5 100mM
Method for crystallization	Detergent micelle	Detergent micelle	Detergent micelle	Detergent micelle
Molecular Construct	1-284, WT, Native	1-284, WT, Native	1-284, WT, Native	1-284, WT, Native
Molecules in ASU	1mol/ASU	4mol/ASU	12mol/ASU	1mol/ASU
Ion binding along 3-fold axis, bound to A69	None	None	None	1 Ca ²⁺
Beamline Facility	APS_24IDC	APS_24IDC	SSRF 19U1	APS_24IDC

Table S3. Data collection and refinement statistics for TRICs structures

Table S3a GgTRIC-A						
	WT_Se	WT_Ca12k	WT_Ca7k	WT_Ca_free	K129A	K129Q
Wavelength (Å)	0.9785	0.9778	1.7712	0.9785	0.9792	0.9792
Bragg spacings (Å)	39.9 - 2.20 (2.28 - 2.20)	41.5 - 1.80 (1.87 - 1.80)	48.5 - 2.0 (2.07 - 1.99)	45.3 - 2.2 (2.28 - 2.20)	41.6 - 2.3 (2.38 - 2.3)	48.49 - 2.4 (2.49 - 2.4)
Space group	P 6 ₃ 2 2	P 6 ₃ 2 2	P 6 ₃ 2 2	F 4 ₁ 3 2	P 6 ₃ 2 2	P 6 ₃ 2 2
Unit cell (Å, °)	127.4 127.4 102.1 90 90 120	126.7 126.7 102.0 90 90 120	127.4 127.4 102.1 90 90 120	268.2 268.2 268.2 90 90 90	127.0 127.0 101.4 90 90 120	127.3 127.3 101.8 90 90 120
Total reflections	954440 (92294)	1462808 (74031)	8559428(635203)	6347974(648863)	892118 (86063)	688343 (77419)
Unique reflections	25405 (2489)	43116 (3169)	33696 (3176)	42385 (4134)	21989 (2140)	17845 (1900)
Multiplicity	37.6 (37.1)	33.9 (23.3)	254.0 (199.2)	149.8 (156.7)	40.6 (40.2)	38.6 (40.7)
Completeness (%)	100.0 (100.0)	95.0 (71.0)	100.0 (97.0)	100.0 (99.3)	99.57 (99.91)	90.94 (99.74)
Mean I/sigma(I)	30.42 (2.11)	33.39 (0.74)	36.65 (0.97)	27.48 (0.81)	27.00 (1.32)	23.15 (1.05)
Wilson B-factor	49.6	40.6	37.6	54.66	52.71	65.54
R-merge	0.105 (2.38)	0.069 (3.84)	0.174 (20.7)	0.293 (13.08)	0.163 (4.14)	0.139 (4.92)
R-meas	0.106 (2.41)	0.070 (3.92)	0.174 (20.7)	0.294 (13.12)	0.165 (4.19)	0.141 (4.98)
R-pim	0.0175 (0.393)	0.0119 (0.777)	0.0109 (1.424)	0.0241(1.043)	0.0259 (0.658)	0.0229 (0.773)
CC1/2	0.999 (0.718)	1 (0.316)	1 (0.361)	0.999 (0.377)	1 (0.565)	0.999 (0.516)
CC*	1 (0.914)	1 (0.693)	1 (0.728)	1 (0.74)	1 (0.85)	1 (0.825)
Reflections used in refinement	25402 (2490)	43014 (3084)	33654 (3162)	42353 (4112)	21920 (2138)	17832 (1895)
Reflections used for R-free	1294 (124)	2198 (145)	1687 (160)	2198 (197)	1118 (108)	906 (94)
R-work	0.192 (0.267)	0.186 (0.375)	0.183 (0.347)	0.255 (0.375)	0.207 (0.301)	0.203 (0.325)
R-free	0.206 (0.289)	0.197 (0.379)	0.204 (0.373)	0.269 (0.376)	0.228 (0.350)	0.230 (0.340)
CC(work)	0.854 (0.845)	0.892 (0.639)	0.859 (0.651)	0.800 (0.526)	0.916 (0.741)	0.783 (0.671)
CC(free)	0.882 (0.801)	0.919 (0.609)	0.884 (0.744)	0.798 (0.464)	0.877 (0.526)	0.881 (0.647)
Number of non-hydrogen atoms	1923	1953	1897	1820	1860	1925
macromolecules	1821	1820	1802	1806	1806	1818
ligands	6	7	6	4	6	6
solvent	96	126	89	10	48	101
Protein residues	226	226	224	225	224	224
RMS ideality (bonds, Å)	0.003	0.017	0.019	0.002	0.002	0.003
RMS ideality (angles, °)	0.46	1.19	1.24	0.4	0.38	0.54
Ramachandran favored (%)	99.6	99.6	99.6	98.7	99.6	99.6
Ramachandran outliers (%)	0	0	0	0	0	0
Rotamer outliers (%)	0	1	0	0.52	0	0
Clashscore	2.19	5.49	3.88	1.67	1.94	2.2
Average B-factor	60.85	50.67	51.56	60.49	65.09	76.03
macromolecules	60.54	49.96	51.33	60.52	65.27	75.75
ligands	60.61	85.69	51	53.09	53.34	59.91
solvent	66.84	59.01	56.22	56.72	59.88	82.03
PDB ID	6IYU	6IYX	6IZF	6IYZ	6IZO	6IZ1

Table S3b XTRIC-B				
	WT_Ca_free1	WT_Ca_free2	WT_Ca_free3	WT_Ca7k
Wavelength (Å)	1.7712	1.7712	0.9778	1.7712
Bragg spacings (Å)	44.2 - 3.7 (3.83 - 3.70)	47.5 - 3.78 (3.92 - 3.78)	49.9 - 3.10 (3.21 - 3.10)	48.1 - 3.29 (3.41 - 3.29)
Space group	F 4 3 2	P 3 2 1	P 4 ₂ 2 ₁ 2	F 4 3 2
Unit cell (Å, °)	250.0 250.0 250.0 90 90 90	190.1 190.1 117.6 90 90 120	290.2 290.2 195.8 90 90 90	250.1 250.1 250.1 90 90 90
Total reflections	279170 (27858)	923906 (79893)	4943816 (556950)	820758 (44824)
Unique reflections	7572 (747)	24623 (2302)	137476 (14935)	9895 (1034)
Multiplicity	36.9 (37.2)	37.5 (34.7)	36.0 (37.3)	82.9 (43.3)
Completeness (%)	98.0 (100)	98.23 (84.06)	90.88 (99.85)	91.4 (86.76)
Mean I/sigma (I)	10.67 (0.36)	9.77 (0.73)	11.98 (1.29)	15.74 (0.39)
Wilson B-factor	146.6	181.64	81.5	154.0
R-merge	0.327 (7.00)	0.239 (10.99)	0.383 (3.87)	0.213 (15.61)
R-meas	0.331 (7.10)	0.243 (11.16)	0.388 (3.93)	0.214 (15.8)
R-pim	0.0542 (1.152)	0.040 (1.888)	0.064 (0.639)	0.0228 (2.37)
CC1/2	0.999 (0.235)	0.999 (0.288)	0.998 (0.52)	0.999 (0.42)
CC*	1 (0.617)	1 (0.669)	1 (0.827)	1 (0.768)
Reflections used in refinement	7467 (668)	24351 (2057)	137158 (14912)	9746 (898)
Reflections used for R-free	334 (40)	1158 (109)	6780 (729)	456 (50)
R-work	0.293 (0.402)	0.291 (0.426)	0.279 (0.379)	0.309 (0.484)
R-free	0.307 (0.376)	0.330 (0.418)	0.299 (0.390)	0.320 (0.532)
CC (work)	0.802 (0.432)	0.806 (0.489)	0.837 (0.529)	0.774 (0.308)
CC (free)	0.643 (0.657)	0.776 (0.556)	0.850 (0.525)	0.683 (0.096)
Number of non-hydrogen atoms	1769	7064	21192	1769
macromolecules	1766	7064	21192	1766
solvent	3	ND	ND	3
Protein residues	224	896	2688	224
RMS ideality (bonds, Å)	0.002	0.002	0.003	0.003
RMS ideality (angles, °)	0.4	0.39	0.44	0.88
Ramachandran favored (%)	97.8	97.3	96.9	96.9
Ramachandran outliers (%)	0.9	1	1	0.9
Rotamer outliers (%)	1.1	1.3	1.6	0
Clashscore	5.95	6.45	5.62	6.8
Average B-factor	134.2	200.5	75.02	158.67
macromolecules	134.31	200.5	75.02	158.75
solvent	65.28	ND	ND	111.86
PDB ID	6IZ5	6IZ3	6IZ4	6IZ6